TABLE III: Vertical Excitation Energies (nm) for Valence Transitions in the Benzenesulfonyl Radical

transition	energy, nm	oscillator strength
$\pi_2(A'') \rightarrow$ SOMO	475	0.007
$\pi_2(A') \rightarrow$ SOMO	450	0.113
$n_1(A'') \rightarrow$ SOMO	355	0.126
$n_2(A'') \rightarrow$ SOMO	315	0.585
SOMO $\rightarrow \pi_3^*(A')$	310	0.015
$n_2(A') \rightarrow$ SOMO	280	0.092
SOMO $\rightarrow \pi_3^*(A'')$	260	0.000
$\pi_1(A') =$ SOMO	240	0.003
$n_1(A') \rightarrow$ SOMO	195	0.181

The calculated vertical transitions for $MeSO_2$ are given in Table II together with their oscillator strengths. The strongest transitions in the UV-visible spectrum—those with the highest oscillator strengths—are valence transitions associated with the SO_2 moiety that involve transfer of electrons from the oxygen atoms to the SOMO. Rydberg transitions between the SOMO and the nearest vacant orbitals, i.e. those with higher principal quantum numbers, have much lower oscillator strengths and are essentially "forbidden" in three cases. For $MeSO_2$ the Rydberg transitions generally occur at higher energies than the dominant valence transitions.

Calculations for $PhSO_2$ are reported in Table III. For simplicity, the Rydberg transitions have been omitted since these are of higher energy than the valence transitions and do not contribute to any significant extent in the experimentally accessible wavelength region. The results show that the phenyl group exerts a small but significant perturbation on the sulfonyl system as is illustrated in Figure 3. In fact, it is the π_2 orbital of the benzene ring which has A' symmetry that interacts with the SOMO and reduces the unpaired spin density on the SO_2 group. The composition of the SOMO is 43% at sulfur (9%, 3s, 26%, 3p, 8% 3d) and 39% at the oxygen atoms with the remainder being largely on the aromatic ring.

Introduction of the phenyl group has three main effects. First, there is a contribution to the spectrum due to valence transitions of the electrons in the π orbitals of the benzene ring to the SOMO. Second, it causes an increase in the oscillator strength of the $n_1(A'')$ to SOMO transition. Third, it increases the energy of the SOMO relative to the n-type orbitals located principally on the oxygen atoms so that while the $n_2(A'')$ to SOMO transition remains dominant, it is blue shifted by 15 nm. The calculated effect of phenyl substitution is therefore in excellent agreement with the wavelength shift observed experimentally.

Conclusion

MSX_α calculations successfully reproduce the experimental UV-visible spectra of sulfonyl radicals. For methanesulfonyl they show that the most important transitions observed in this region are valence transitions involving transfer of electrons from the lone pair orbitals of the oxygen atoms to the SOMO. Replacement of the methyl by a phenyl group introduces additional valence transitions from the π orbitals of the benzene ring to the SOMO and sightly destabilizes the SOMO with respect to the other molecular orbitals. As a consequence the dominant transition remains an oxygen to SOMO but is blue shifted by 15 nm in excellent agreement with experiment.

Acknowledgment. We thank Drs. M. Tamba and A. Castelhano for their help in measuring spectra of some of the sulfonyl radicals described in this work.

Structure and Excited-State Dynamics of 2-Aminopyridine van der Waals Molecules and Hydrogen-Bonded Complexes

James W. Hager, Gary W. Leach, David R. Demmer, and Stephen C. Wallace*

Department of Chemistry, University of Toronto, Toronto, Ontario, Canada M5S 1A1
(Received: December 17, 1986; In Final Form: March 10, 1987)

We report the results of experimental and theoretical investigations of the electronic spectroscopy, binding energies, and excited-state dynamics of 2-aminopyridine (2AP) van der Waals and hydrogen-bonded complexes. For the argon and methane van der Waals molecules, we have determined the binding energies of the ground and first excited electronic states of the neutral species as well as for the ground state of the $2AP^+$–Ar and 2AP–CH_4 ionic complexes. Results from two-color threshold photoionization studies of selected vibronic levels of 2AP–Ar and 2AP–CH_4 provide insight into the competition between vibrational predissociation, intramolecular vibrational redistribution, and photoionization. Mechanisms of dissociation of these complexes based on these results are presented and discussed. For the 2AP hydrogen-bonded complexes involving water, methanol, and ethanol, vibrational predissociation was monitored via photoionization and fluorescence lifetime technniques. Photodissociation thresholds have been obtained for these hydrogen-bonded complexes directly providing bond energies. Potential energy calculations performed on these complexes suggest that the excited-state arrangement is cyclic with two hydrogen bonds. We also report the observation of the 2AP dimer which displays an extremely large spectral shift to lower energies. The origin of the large excited-state stabilization of the 2AP dimer and the 2AP–ROH complexes is also discussed.

Introduction

Small molecular complexes such as van der Waals molecules and hydrogen-bonded clusters have received considerable attention in recent years.[1] When prepared ultracold in a supersonic expansion, these species have proven to be excellent systems in which to investigate both intermolecular interactions and molecular dynamics. In a previous publication,[2] we reported the electronic spectra and fluorescence decay characteristics of complexes of 2-aminopyridine (2AP) with argon and methane as well as with the hydrogen-bonding partners water, alcohols, ammonia, and dioxane. We observed[2] a considerable lengthening of the 2AP excited-state lifetime upon hydrogen-bond formation which was

(1) McKellar, A.; Robert, W. *Faraday Discuss. Chem. Soc.* **1982**, *73*, 89.

(2) Hager, J. W.; Wallace, S. C. *J. Phys. Chem.* **1985**, *89*, 3833.

0022-3654/87/2091-3750$01.50/0

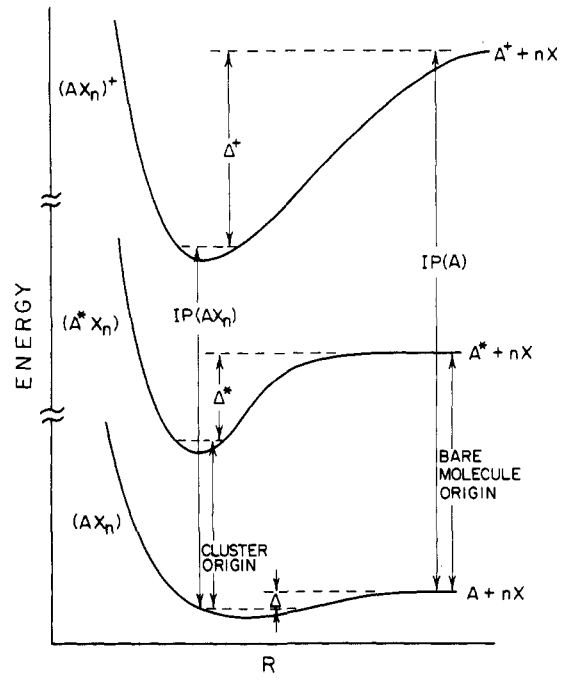

Figure 1. Simplified potential energy curves for the ground and excited states of the neutral van der Waals molecule AX_n and for the ground ionic state of A^+X_n. The binding energies of these species are represented as Δ for the neutral ground state; Δ^* for the neutral excited state; and Δ^+ for the ionic ground state.

attributed to the effects of site-specific hydrogen-bonding pairwise interactions on the excited-state singlet–triplet coupling. In the current paper, we explore the bond energies and dissociation dynamics of excited-state 2AP-Ar and CH_4 van der Waals molecules and the hydrogen-bonded complexes involving water, methanol, and ethanol using fluorescence and photoionization techniques. In addition, we report the observation of the 2AP dimer and examine the source of the very large excited-state stabilization energy of the dimer relative to the 2AP monomer.

Photodissociation of a van der Waals molecule can occur if the energy content of the excited vibronic band is greater than the complex binding energy. If the vibrational predissociation rate constant is of the order of that of the experimental observable, e.g., fluorescence or ionization, dissociation products can be observed. Of particular interest is the magnitude of the rate of the predissociation process, the internal energy content of the resulting polyatomic fragment, and the degree to which vibrational predissociation competes with the other dynamical processes of the electronically excited van der Waals molecule, such as intramolecular vibrational redistribution (IVR). Furthermore, using the excited-state binding energies of the complexes together with the measured values of the electronic spectral shifts and the adiabatic ionization potentials of the complexes, one can determine the cluster binding energies in the neutral and ionic ground electronic states. This is illustrated in Figure 1. When coupled with intermolecular potential calculations, these binding energies can provide insight into the intermolecular interaction energies and geometry changes upon electronic excitation and ionization. This can be of considerable use when confronted with complicated electronic and threshold photoionization spectra.

The experimental techniques we have employed in these investigations are nanosecond and picosecond laser-excited fluorescence lifetime measurements, mass-selected photoionization excitation spectroscopy, and two-color threshold photoionization spectroscopy. Mikami et al.[3] have recently demonstrated that two-color threshold photoionization spectroscopy can be a very sensitive method for probing the predissociation dynamics of electronically excited van der Waals molecules. Here, the first laser selectively excites the complex to a well-defined level and the second laser ionizes the complex. As demonstrated by us[4] and others,[3,5] excited-state dynamical processes occurring on a time scale faster than the ionization rate, such as radiationless decay and IVR, will be reflected in the threshold photoionization spectrum. Thus, if the complex dissociates with a rate much greater than the ionization rate, only ions corresponding to the ionization of electronically excited fragments will be detected. Since van der Waals complexes have ionization potentials at lower energies than the fragments, the identity of the species (complex or fragment) being ionized can readily be determined from the position(s) of the ionization threshold(s). As has been noted by Mikami et al.,[3] it is important to realize that the ionization step in this two-color scheme is an absorption process, and thus much faster than fluorescence. Consequently, this technique has the potential for detecting short-lived complexes which cannot be detected by fluorescence.

In the present study, we have found that two-color threshold photoionization spectroscopy of 2AP–Ar and 2AP–CH_4 is an extremely sensitive technique for probing vibrational predissociation, vibrational relaxation, and fragment vibrational energy content. For the water and alcohol hydrogen-bonded 2AP complexes, we have employed fluorescence lifetime measurements in order to determine energy thresholds for the dissociation of these more strongly bound species. These energy thresholds have been confirmed by measuring the breakoff in complex ion production in the mass-selected photoionization excitation spectra. Coupling experimental results with intermolecular potential calculations has aided in the interpretation of the energetics and dynamics of the 2AP electronically excited complexes. Such investigations provide considerable insight into the early stages of solvation of the chemically important pyridine nucleus.

Experimental Details

A. Laser Photoionization and Fluorescence Studies. The investigations reported here involve the use of fluorescence excitation spectroscopy, nanosecond and picosecond laser excited fluorescence lifetime measurements, one-color photoionization excitation spectroscopy, and two-color photoionization threshold spectroscopy. Most of the apparatus employed has been described previously,[2,4,6] so only brief descriptions will be given here.

For the laser-induced fluorescence studies, the laser light crossed a continuous helium free jet expansion containing 2-aminopyridine vapor and that of the appropriate complexing partner. Either a 50-μm pinhole (P_0 = 15 atm) or a 100-μm pinhole (P_0 = 4 atm) was used as the expansion orifice.

For the nanosecond fluorescence investigations, the excitation light was produced by a Nd:YAG (Quanta Ray DCR 1A) pumped dye laser (Quanta Ray PDL-1) frequency doubled in KD*P (Quanta Ray WEX-1). The resulting line width in the UV was approximately 0.2 cm^{-1} with pulse energies of about 5 mJ which was reduced to $\sim$100 μJ with neutral-density filters. Nanosecond fluorescence lifetime measurements were made with a RCA 4840 photomultiplier and a Tektronix 7912 AD transient digitizer with a dedicated 4052 microcomputer. Each decay was averaged 400 times and base line corrected.

Picosecond excited fluorescence lifetimes were obtained by using the time-correlated single photon counting technique and the light from a frequency-doubled picosecond laser system. Briefly, the output of a mode-locked Nd:YAG laser (Spectra Physics Series 3000) synchronously pumped a cavity dumped dye laser (Spectra Physics Model 375B dye laser and 344 cavity dumper). The dye laser output was frequency doubled in either KD*P or $LiIO_4$ and used to excite the jet-cooled monomer or its complexes. The resulting fluorescence was detected at right angles by a fast microchannel plate PMT (Hamamatsu 1564U-02). UV cutoff filters were used to reject scattered light when this was a problem.

(3) Mikami, N.; Sugahara, Y.; Ito, M. *J. Phys. Chem.* **1986**, *90*, 2080.

(4) Smith, M. A.; Hager, J. W.; Wallace, S. C. *J. Phys. Chem.* **1984**, *88*, 2250.

(5) Fuji, M.; Ebat, T.; Mikami, N.; Ito, M. *J. Phys. Chem.* **1984**, *88*, 4265.

(6) Hager, J. W.; Demmer, D. R.; Wallace, S. C. *J. Phys. Chem.* **1987**, *91*, 1375.

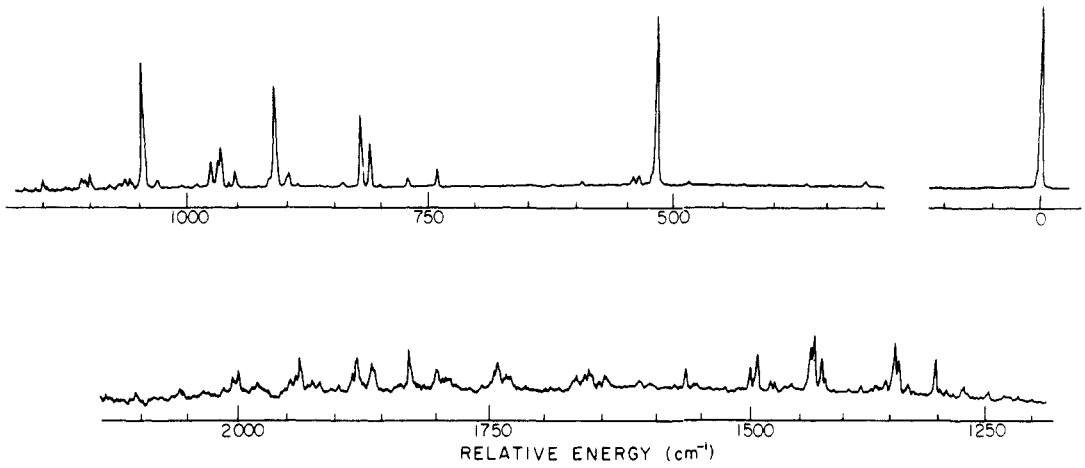

Figure 2. Fluorescence excitation spectrum of jet-cooled 2AP. The expansion conditions were P_0 = 3 atm of helium and D = 100 μm.

The overall temporal resolution of the system is approximately 100 ps (fwhm), so that fluorescence lifetimes were extracted from the decays by a simple least-squares fitting program.

The details of the apparatus for the photoionization studies can be found in earlier publications[4,7] from this group. In the one-color excitation experiments, frequency-doubled light from the nanosecond pulsed Nd:YAG pumped dye laser described above was used as the ionization source. The ions produced in the laser–free jet interaction region are accelerated into a quadrupole mass spectrometer housing with a very small accelerating voltage (<1 V/cm) where they are focused, mass analyzed, and detected with a gain of about 10^5. Signal from the multiplier anode was sent to a gated current integrator (Quanta Ray DGA-1) which detects ion signal strengths during the 500 μs immediately following the laser pulse.

For the two-color studies, the intermediate electronic level in the two-color scheme was prepared by using the light from a XeCl (Lumonics 860-T) pumped dye laser (Lumonics EPD 330) frequency doubled in KD*P. This provided ~1-mJ, 7-ns pulses. Typically the pulse energy was reduced to <~100 μJ to avoid one-color ionization. The ionizing laser light was provided by the frequency-doubled pulsed nanosecond Nd:YAG pumped dye laser described above. The pulse energy of this laser was maintained at approximately 1 mJ and we estimate the ionization rate to be about 10^9 s^{-1}. The two laser beams were sent through the supersonic expansion chamber in a coaxial, counterpropagating fashion. In the current studies, the delay between the arrival of the state preparation and the ionization laser pulses in the interaction region was minimized with a variable delay generator.

The two-color threshold photoionization spectra were obtained with the quadrupole operating in the rf-only mode. This results in detection of total ions with an increase in sensitivity of >100. The identities of the ionized species were determined by comparison of threshold positions with mass-selected two-color spectra and by obtaining mass spectra at various ionizing laser wavelengths.

The data acquisition and sample handling techniques were the same as previously described. The complexing partner concentration in the present study is approximately 0.3 to 1% in helium. 2-Aminopyridine (99+%) was obtained from Aldrich and used without further purification. The samples of the various complexing partners were as previously reported.

B. Potential Energy Calculations. In order to obtain stable cluster geometries and estimates of the cluster binding energies, potential energy calculations were performed. The model considers the pairwise interaction between each atom of the clustering partner and each atom of the parent molecule (with three-body and higher interactions neglected). When the interaction is dominated by dispersive forces the potential energy between atom i of the clustering partner and atom j of the parent molecule is of the Lennard-Jones (6–12) form[8]

$$E_{ij}^{LJ} = \frac{A^{kl}}{r_{ij}^{12}} - \frac{C^{kl}}{r_{ij}^{6}} \qquad (i,j \text{ dispersion interactions})$$

where A^{kl} and C^{kl} are the potential parameters for atoms of type k and l. When the interaction between atoms i and j is dominated by hydrogen-bonding forces the form of the interaction energy is a hydrogen-bonding (10–12) potential:[8]

$$E_{ij}^{HB} = \frac{B^{kl}}{r_{ij}^{12}} - \frac{D^{kl}}{r_{ij}^{10}} \qquad (i,j \text{ hydrogen-bonding interactions})$$

The parameters B^{kl} and D^{kl} are the hydrogen-bonding parameters between atoms of type k and l. The potential parameters for both the Lennard-Jones and hydrogen-bonding interactions were obtained from the work of Scheraga et al.[8] on the empirical potentials in crystals. The total interaction energy is the sum of these interaction energies for all pairs i,j.

$$E_{tot} = \sum_{i=1}^{m}\sum_{j=1}^{n} E_{ij}^{LJ} + E_{ij}^{HB}$$

It should be noted that this energy does not take into account electrostatic interactions between pairs of atoms i,j due to the atomic partial electronic charge. Since reliable partial charges for the molecules studied here are not available, an estimate of the electrostatic interaction was obtained by considering the dipole–dipole interactions for the polar complexes. The magnitude of the electrostatic contribution to the total interaction energy was calculated by using experimental value for the 2AP dipole moment[9] and those of the various complexing partners.[10] The electrostatic contributions determined in this manner were small, being about 7% of the total interaction energy. Consequently, these electrostatic contributions have been neglected in our treatment.

Results and Discussion

A. Jet-Cooled 2-Aminopyridine. The fluorescence excitation spectrum of jet-cooled 2AP is shown in Figure 2. Rotational contour analysis[11] of the $\tilde{A}$–$\tilde{X}$ electronic band system has shown that the transition moment is polarized in the molecular plane and thus to a π,π^* electron promotion. Spectroscopically, this electronic state shows a remarkable similarity to the lowest energy electronic transition of aniline.[12,13] The ground state of both

(7) Smith, M. A.; Hager, J. W.; Wallace, S. C. *J. Chem. Phys.* **1984**, *80*, 3097.

(8) Nemehy, G.; Pottle, M. S.; Scheraga, H. A. *J. Phys. Chem.* **1983**, *87*, 1883.

(9) Kydd, R. A.; Mills, I. M. *J. Mol. Spectrosc.* **1972**, *42*, 320.

(10) *CRC Handbook of Chemistry and Physics*; Weast, R. C., Ed.; CRC Press: West Palm Beach, FL, 1979.

(11) Hollas, J. M.; Kirby, G. H.; Wright, R. A. *Mol. Phys.* **1970**, *18*, 327.

TABLE I: Band Positions, Assignments, and Fluorescence Lifetimes of Jet-Cooled 2-Aminopyridine

rel position, cm^{-1}	assignment	lifetime, ns
0–629	21_1^0	
0–560	22_1^0	
0–375	I_2^0	
0	0_0^0	1.89
523	22_0^1	1.71
540	21_0^1	
815		
824	20_0^1	1.80
911	I_0^2	1.91
967	19_0^1	1.74
972		
978		
1045	22_0^2	1.71
1047	18_0^1	1.74
1304	$978 + 29_0^1$	
1344		
1347	$20_0^1 22_0^1$	1.61
1420		
1433		1.51
1493	$19_0^1 22_0^1$	
1510		
1569	22_0^3 or $18_0^1 22_0^1$	1.69
1731	$20_0^1 I_0^2$	
1797	$19_0^1 20_0^1$	1.72
1826	I_0^4	

molecules is nonplanar about the amino nitrogen, while the first excited states are planar or very nearly planar. Consequently, there is significant activity of the inversion mode upon electronic excitation. On the basis of the work of Hollas et al.[12] and Gordon et al.,[13] we have demonstrated[2] that the $\tilde{A}$–$\tilde{X}$ absorption spectrum can be easily assigned under the assumption of separable vibrational modes with little interaction between these modes. Furthermore, there are several vibrational hot bands that can be observed even under supersonic expansion conditions. Band positions and assignments for the 2AP monomer are presented in Table I.

We have measured the fluorescence lifetimes of jet-cooled 2AP using picosecond laser excitation. These results can also be found in Table I. The band origin of the $\tilde{A}$ state is characterized by a fluorescence lifetime of 1.89 ns with a very slow reduction in decay time as a function of excess vibrational energy. Although direct measurements of the fluorescence quantum yield of 2AP vapor have not been performed, one can estimate the radiative lifetime from the oscillator strength of this transition.[14] Taking the f value of 0.072, we obtain a radiative lifetime of approximately 19 ns. Using the measured fluorescence lifetime of 1.89 ns, the quantum yield of fluorescence can be estimated to be about 0.1. The origin of this relatively low quantum yield has been discussed in detail earlier,[2] but will be mentioned briefly here since it also relates to the present work.

The first excited singlet and triplet states of 2AP are π,π^* states.[15] At somewhat higher energies in the triplet manifold, but lower in energy than the first $^1\pi,\pi^*$ state, is an n,π^* triplet state.[16] Thus, there is a strong spin–orbit coupling between the $^1\pi,\pi^*$ and $^3n,\pi^*$ states leading to significant intersystem crossing upon optical excitation and the much less than unity fluorescence quantum yield. It should be noted that this singlet–triplet coupling is extremely sensitive to the relative energies of the $^1\pi,\pi^*$ and $^3n,\pi^*$ states. This provides us with an excellent system with which to probe solvent-induced perturbations to the parent molecule energy levels.

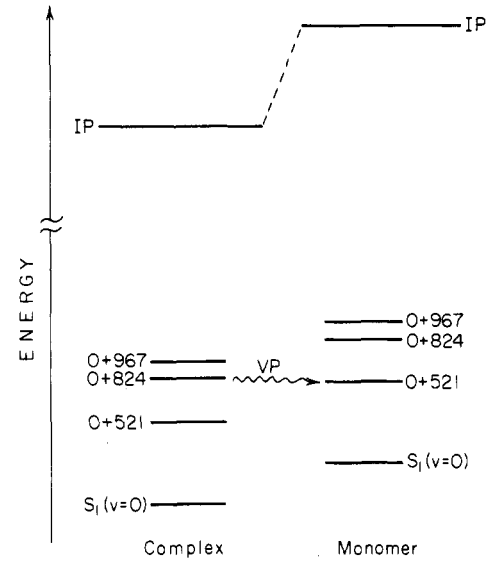

Figure 3. Mass-selected two-color photoionization spectra of (a) 2AP–Ar and (b) 2AP–CH_4. The energy scale is relative to the bare 2AP origin position. The ionizing laser was tuned to approximately 50 cm^{-1} above the IP of the respective complex. Helium containing a small amount of the complexing partner (<1%) was used as the carrier gas. The expansion conditions were P_0 = 2.8 atm. and D = 100 μm.

B. Argon and Methane van der Waals Molecules. 1. Binding Energies. Formation of van der Waals molecules between 2AP and the complexing partners argon and methane leads to a reduction in the transition energy which is approximately proportional to the polarizability of the respective complexing partner. This demonstrates that dispersion and dipole–induced dipole intermolecular interactions are responsible for the binding of these clusters. Figure 3 presents the mass-selected photoionization spectra of these two complexes. The measured spectral shifts for 2AP–Ar and 2AP–CH_4 are −32 and −68 cm^{-1}, respectively. In each system, we have also identified an intermolecular vibrational excitation. For 2AP–Ar this van der Waals frequency is 18 cm^{-1} and for 2AP–CH_4, 28 cm^{-1}. It is reasonable to assign these to the respective van der Waals stretch vibrations.

We have measured the fluorescence lifetimes of the band origins of 2AP–Ar and 2AP–CH_4 in order to determine the degree to which the van der Waals partner perturbs the radiative properties, and the $^1\pi,\pi^*/^3n,\pi^*$ coupling, of the parent molecule. The values we have obtained are 1.80 ns for 2AP–Ar and 1.92 ns for 2AP–CH_4. Consequently, these two van der Waals molecules are examples of systems in which the solvent partners do not significantly perturb the spectroscopy or dynamics of the chromophore and can be considered to be truly inert.

In order to determine the ground-state binding energies of 2AP–Ar and –CH_4, we have investigated the electronic spectra of these complexes associated with several hot vibrational transitions. In general, if the ground-state vibrational energy exceeds the complex binidng energy, the van der Waals molecule will predissociate prior to reaching the laser–jet interaction volume. Thus, the absence of van der Waals molecule absorption features associated with a series of hot bands which terminate at the vibrationless level of the excited state aids in the determination of upper limits to the complex binding energy in the ground electronic state.

The hot bands of interest in this study are 21_1^0 (0 − 629 cm^{-1}), 22_1^0 (0 − 560 cm^{-1}), and I_2^0 (0 − 375 cm^{-1}). No argon or methane van der Waals molecule features could be observed for the 21_1^0 transition, while 2AP–CH_4 transitions associated with 22_1^0 and I_2^0 were readily detected. This allows us to bracket the ground-state binding energy of 2AP–CH_4 as 560 $cm^{-1} < D_0 < 629$ cm^{-1}, and from the relationship[11]

$$D_0(S_1) = D_0(S_0) + \Delta\nu \quad (1)$$

where $\Delta\nu$ is the electronic spectral shift, the excited-state binding energy, 628 $cm^{-1} < D_0 < 697$ cm^{-1}. For 2AP–Ar, we were unable

(12) Hollas, J. M.; Musa, H.; Ridley, T. *J. Mol. Spectrosc.* **1984**, *104*, 89.
(13) Gordon, R. D.; Clark, D.; Crawley, J.; Mitchell, R. *Spectrochim. Acta, Part A* **1984**, *40A*, 657.
(14) Inuzuka, K.; Fujimoto, A. *Spectrochim. Acta, Part A* **1986**, *42A*, 929.
(15) (a) Motten, A. G.; Kwiram, A. L. *J. Chem. Phys.* **1981**, *75*, 2608. (b) Hotchandani, S.; Testa, A. C. *J. Chem. Phys.* **1973**, *59*, 596.
(16) Kimura, K.; Takaoka, H.; Nagai, R. *Bull. Chem. Soc. Jpn.* **1977**, *50*, 1343.
(17) Levy, D. H. *Adv. Chem. Phys.* **1981**, *47*, 323.

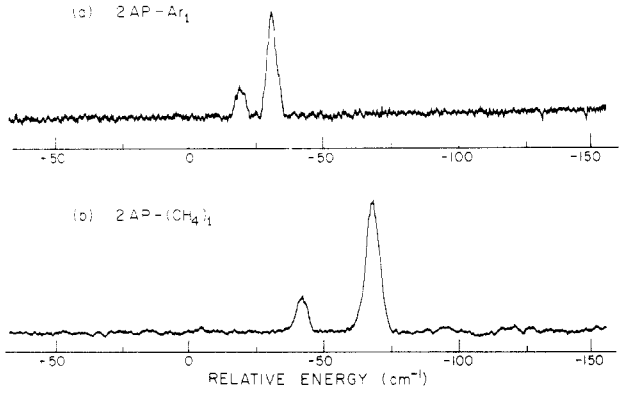

Figure 4. Potential energy diagram showing the approximate level positions of the 2AP–Ar van der Waals molecule with respect to those of the 2AP monomer.

to locate any van der Waals molecule transitions associated with any of these hot bands, and we therefore tentatively place $D_0 <$ 375 cm^{-1} for the ground state and $D_0 <$ 407 cm^{-1} for the excited state of 2AP–Ar.

2. Excited-State Vibrational Predissociation Dynamics. If van der Waals molecules are excited to vibronic levels higher in energy than the binding energy of the complex, vibrational predissociation can occur as illustrated in Figure 4. We have also employed two-color threshold photoionization as a technique to probe the vibrational predissociation dynamics of 2AP*–Ar and 2AP*–CH_4. In these studies, the clusters are excited above D_0 by the first laser, while the second laser ionizes all excited-state species in the expansion. Since the first laser excites the van der Waals molecules above their respective binding energies, one expects vibrational predissociation to be competitive with ionization. Consequently, the second laser will produce predominantly $2AP^+$. Mikami et al.[3] have demonstrated that, in favorable cases, the position(s) of the ionization threshold(s) can provide new information regarding vibrational predissociation dynamics. Of particular interest is the degree of vibrational excitation in the 2AP* fragment, as well as the extent to which vibrational predissociation (VP), complex vibrational relaxation (IVR), and ionization compete.

Figure 5 displays the threshold photoionization spectra of 2AP–Ar and 2AP–CH_4 ionized from the 0 + 824 cm^{-1} (20_0^1) level. In both spectra there is more than one threshold. For 2AP–CH_4 (Figure 5a), mass analysis shows that the smaller, lower energy threshold is due to ionization of the cluster. The energy of this ionization onset corresponds exactly to the minimum energy for ionization of 2AP–CH_4($\bar{\nu}$=824 cm^{-1}) and reflects an ionization potential stabilization energy of 370 cm^{-1}, in excellent agreement with our earlier results.[2] Thus, there is a small amount of undissociated complex present, even when excited at least 127 cm^{-1} above D_0. The second threshold is due to production of $2AP^+$ and the threshold energy corresponds to the adiabatic ionization potential plus the vibrational energy content of the excited state, i.e., IP_0 + 824 cm^{-1}. This strongly suggests that, upon dissociation, the major product is 2AP(S_1;v'=0).

The threshold spectrum of 2AP–Ar(0+824 cm^{-1}) in Figure 5b consists of three ionization onsets. Again, the lowest energy onset corresponds to the minimum energy required for ionization of the complex and shows an ionization potential stabilization of 170 cm^{-1}. At the energy corresponding to this threshold $2AP^+$–Ar was detected in the mass spectrometer.

The two higher energy thresholds can be best understood through comparison with threshold spectra of isolated 2AP. When corrected for differences in the first photon energy, the relative threshold position for a series of 2AP monomer vibrational levels merely reflects the difference in the vibrational frequencies of each vibration between the S_1 and ground electronic state of the ion.[7] This arises because of the strong propensity for Δv = 0 ionizing transitions for isolated 2AP.[2] The only exception in the low energy region that we find is for the 22^1 level. As shown in Figure 6, ionization from the 22^1 level produces significant Δv = −1 intensity

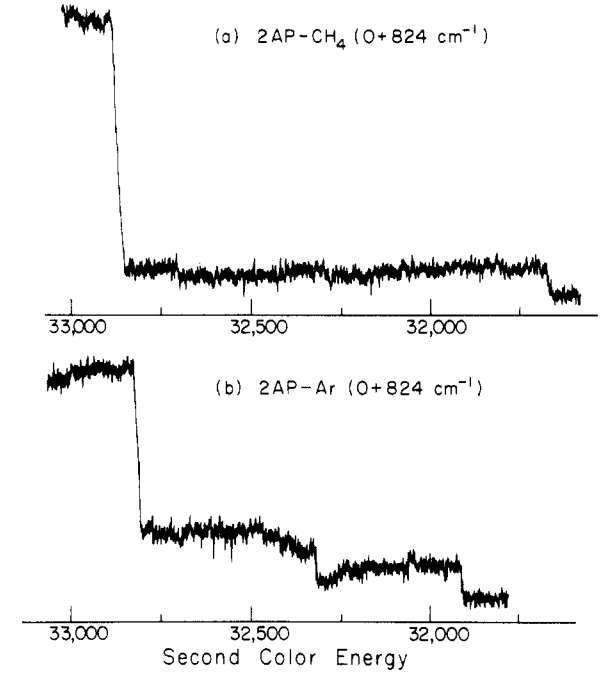

Figure 5. Threshold photoionization spectra of (a) 2AP–CH_4 and (b) 2AP–Ar following excitation to the 0 + 824 cm^{-1} (20_0^1) level of the complex. The wavelength scale corresponds to the ionizing laser wavelength.

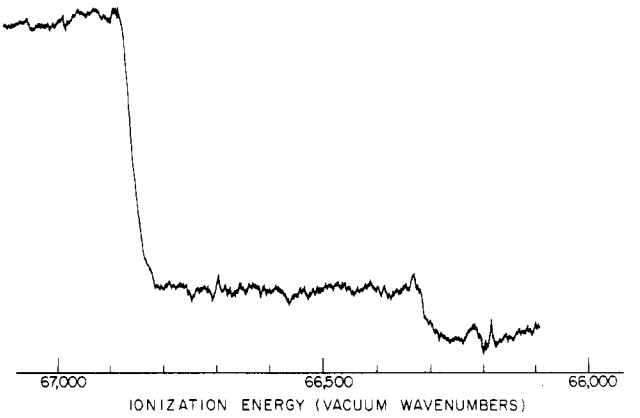

Figure 6. Threshold photoionization spectrum of the 2AP monomer following excitation to the 0 + 523 cm^{-1} (22_0^1) level. The wavelength scale is the total two-color energy.

as well as the more common Δv = 0. Comparison of this spectrum with that of 2AP–Ar(v'=824 cm^{-1}) in Figure 5b shows striking similarity with the exception of the cluster ion threshold (the lowest energy onset) and shows that 2AP(S_1; 22^1) is the major fragment from complex dissociation. Analysis of the threshold intensity for several spectra indicates that at least 90% of the dissociated 2AP is formed in the 22^1 level.

The threshold photoionization spectra of 2AP–Ar and –CH_4 ionized from the S_1;0+824 cm^{-1} level are quite similar. For both van der Waals molecules there is evidence of a small amount of undissociated complex. Consequently, the rate of vibrational predissociation is only slightly greater than the rate of ionization. The ionization rate in these experiments has been estimated to be approximately 10^9 s^{-1} and this gives a lower limit for the predissociation rate at this energy of $>10^9$ s^{-1}. Furthermore, it should be noted that there are no signs of extensive cluster vibrational redistribution in these two photoionization spectra which would be characterized by very gradual ionization onsets representative of photoionization from many vibronic levels.[3-5]

The production of 2AP(S_1;v'=22^1; 0+523 cm^{-1}) upon dissociation of 2AP–Ar(0+824 cm^{-1}) allows the more accurate placement of the upper limit of the excited-state complex binding

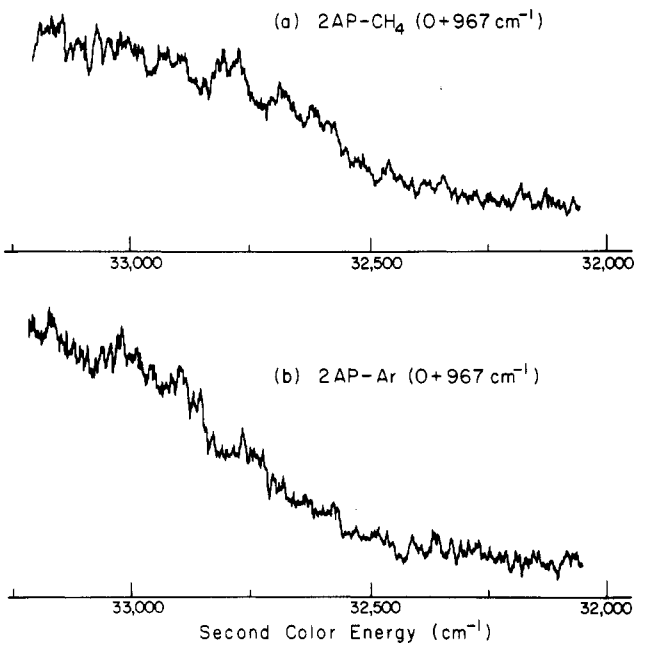

Figure 7. Threshold photoionization spectra of (a) 2AP–CH_4 and (b) 2AP–Ar following excitation to the 0 + 967 cm^{-1} (19_0^1) level of the complex. The wavelength scale corresponds to the ionizing laser wavelength.

energy as $D_0 < 301$ cm^{-1}, consistent with the hot band results. Using this value we are also able to place an upper limit on the binding energy of $2AP^+$–Ar. The binding energy of the complex ion can be obtained from the relation[18]

$$D_0(2AP^+\text{–Ar}) = D_0(2AP\text{–Ar}) + \Delta IP_0 \qquad (2)$$

where ΔIP_0 is the ionization potential stabilization due to complex formation. In a previous publication,[2] we measured the ΔIP_0 for this complex to be −175 cm^{-1}. Using the ground-state binding energy upper limit of $D_0 < 269$ cm^{-1}, one obtains a value of $D_0 < 444$ cm^{-1} for $2AP^+$–Ar. Thus, the ionic complex is approximately 65% more tightly bound than the ground state of the neutral molecule.

Figure 7 displays the threshold photoionization spectra of 2AP–Ar and 2AP–CH_4 ionized from the S_1;0+967 cm^{-1} (19_0^1) band. There are several points to note about these spectra. Firstly, for both van der Waals systems, the only ion that could be detected is $2AP^+$. This demonstrates that vibrational predissociation occurs at a rate which is much faster than ionization. Secondly, the very broad thresholds in these spectra are characteristic of ionization from a distribution of 2AP levels.[3-5] The most likely way by which such a distribution can be prepared in a process such as this is via rapid vibrational redistribution prior to dissociation. These results, then, are consistent with a picture in which cluster IVR populates levels of the van der Waals molecule which then undergo vibrational predissociation. Similar observations have been made by Mikami et al.[3] employing threshold ionization of vibronically excited pyrimidine–Ar.

In general, the values of the complex bond energies constitute upper limits to D_0, since in order to observe dissociation, one must be in the energy regime where complex dissociation occurs on a time scale fast with respect to that of the experimental observable of interest (e.g., fluorescence, ionization). The results obtained for the 2AP–Ar and –CH_4 complexes at the 0 + 824 and 0 + 967 cm^{-1} levels are interesting with respect to this competition. At the higher energy excitation, the two-color threshold spectrum indicates that extensive vibrational redistribution of the complex occurs prior to dissociation, resulting in the population of a distribution of 2AP levels which are then ionized. This is not unexpected considering the many low-frequency modes associated with the van der Waals bond and the rapid increase in state density

(18) Jortner, J.; Even, U.; Leutwyler, S.; Berkovitch-Yellin, Z. *J. Chem. Phys.* **1983**, *78*, 309.

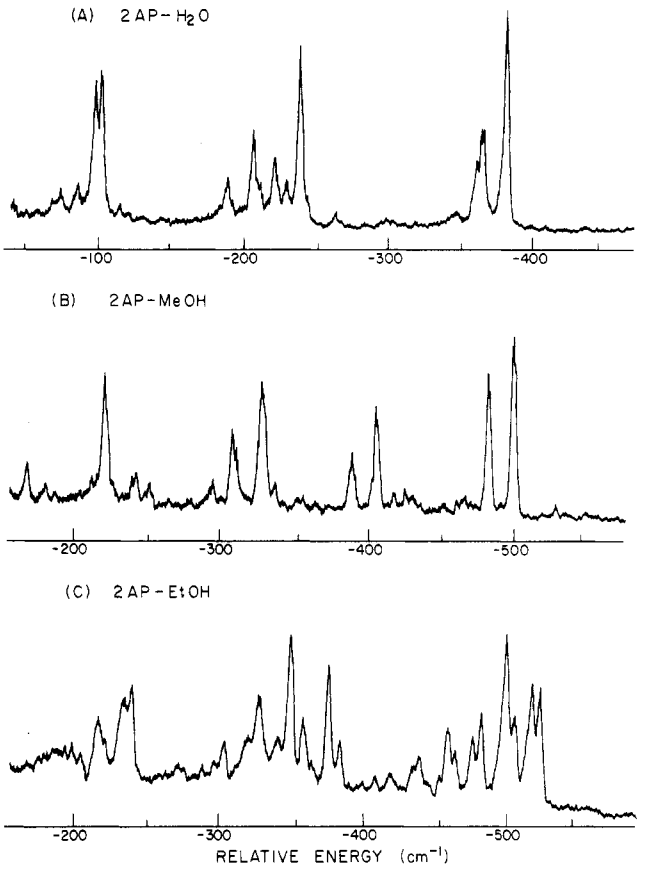

Figure 8. Mass-selected two-color photoionization spectra of the low energy electronic transitions of (a) 2AP–H_2O, (b) 2AP–MeOH, and (c) 2AP–EtOH. The ionizing laser was tuned to approximately 200–300 cm^{-1} above the IP of the respective complex. The expansion conditions were P_0 = 10 atm of helium and D = 50 μm.

as a function of excess energy. Thus, extensive cluster IVR is the dominant dynamical process at this excitation energy for both 2AP–CH_4 and 2AP–Ar resulting in the population of many vibronic levels from which dissociation takes place.

An example of much different excited-state dynamics is reflected in the threshold photoionization spectra of the 0 + 824 cm^{-1} level. Here, we have presented evidence of dissociation which populates predominantly a single excited-state level of the bare molecule with no sign of the extensive vibrational redistribution occurring prior to dissociation. One must realize however that for predissociation to occur there must be limited IVR in the sense that energy must flow from the initially prepared level to the van der Waals stretch.

Mikami et al.[3] have provided evidence that vibrational predissociation of pyrimidine–argon van der Waals complexes can occur by two processes, one "direct" and the other "indirect". The direct mechanism involves complex dissociation from the initially excited level. Consequently, the product distribution reflects only the dissociation dynamics of this initially excited level. These workers have also shown the presence of a second, indirect mechanism in which dissociation occurs from vibronic states populated by extensive vibrational redistribution of the cluster.

This vibrational predissociation picture fits our 2AP results very well. Vibrational predissociation of 2AP–CH_4 and 2AP–Ar(v' = 824 cm^{-1}) is consistent with the direct mechanism whereby vibrational predissociation is the predominant excited-state dynamical process. This stands in contrast to the dynamics of these complexes at the 0 + 967 cm^{-1} level discussed above in which the indirect predissociation process occurs by way of the many complex states populated via vibrational redistribution.

C. Hydrogen-Bonded Complexes: 2AP–H_2O, –MeOH, –EtOH. 1. Hydrogen-Bond Strengths. The electronic spectra of hydrogen-bonded 2AP complexes are substantially more complicated than those discussed above. The mass-selected pho-

TABLE II: Band Positions and Vibrational Excitations of 2AP Hydrogen-Bonded Complexes

complex	$\Delta\nu$, cm^{-1}	complex vibrnl freq, cm^{-1}
2AP–H_2O	−386	8
		17
		32
		143
2AP–MeOH	−503	17
		94
2AP–EtOH	−518	5
		18
		146
2AP dimer	−1668	7
		30
		45
		100
		156

toionization spectra of the 1:1 hydrogen-bonded complexes of 2AP with water, methanol, and ethanol are shown in Figure 8. The excited-state stabilization energies for these species have all been found[2] to be greater than 350 cm^{-1}. Electronic spectral shifts and intermolecular vibrational frequencies are compiled in Table II. These large spectral shifts indicate a substantial strengthening of the hydrogen bond upon optical excitation leading to changes in equilibrium geometries and the observed activity of the hydrogen-bond stretch, bend, and, in the case of the ethanol complex, torsional motions.

In an earlier publication,[2] we demonstrated that the fluorescence lifetimes of these 2AP hydrogen-bonded complexes are significantly different from that of the bare molecule. For the electronic origins of 2AP–H_2O, the fluorescence lifetime was found to be 12.6 ns, for 2AP–MeOH 19.3 ns, and for 2AP–EtOH 21.4 ns. This dramatic lengthening of the fluorescence lifetime has been suggested[2] to be due to changes in the $^1\pi,\pi^*/^3n,\pi^*$ energy gap for the complex and an associated decrease in the singlet–triplet coupling and importance of intersystem crossing. The effect of hydrogen bonding therefore is to alter significantly the relative electronic state energies and effectively remove an efficient nonradiative channel, thus enhancing the fluorescence quantum yield. Within this picture, the strength of the hydrogen bond, and thus the perturbation to the 2AP chromophore, is related to the change in the fluorescence lifetime.

The changes in fluorescence lifetime also provide an excellent tool for probing the bond strengths of these hydrogen-bonded complexes. Increasing the vibrational excitation of the complex by exciting to higher energies within S_1 will eventually lead to sufficient energy to break the hydrogen bond. When the dissociation rate is fast enough to compete with the fluorescence rate, one should be able to detect the onset of monomerlike fluorescence lifetimes. This can be represented as

$$\text{2AP-X}(S_0) \xrightarrow{h\nu} \text{2AP-X}(S_1;\ \nu) \xrightarrow{VP} \text{2AP}(S_1;\ \nu'<\nu)$$

$$\downarrow -h\nu' \qquad\qquad \downarrow -h\nu''$$

$$\tau(\text{long}) \qquad\qquad \tau(\text{short})$$

Thus, in the case of 2AP–MeOH, the signature of cluster fluorescence will be emission with a long lifetime, whereas fragment fluorescence following rapid predissociation will be characteristically short.

In Figure 9 the observed fluorescence lifetimes of the bare molecule and several 1:1 complexes are plotted as a function of increasing energy in the first excited singlet state. For the water, methanol, and ethanol complexes, there are distinct thresholds at which the fluorescence decay times become dramatically shorter. These thresholds represent the energies at which vibrational predissociation effectively competes with the fluorescence rates allowing the detection of 2AP* emission and thus can be considered to be upper limits to the respective hydrogen-bond energies. For 2AP–H_2O, we obtain a value of $D_0 < 1347$ cm^{-1} and for 2AP–MeOH and –EtOH, $D_0 < 1569$ cm^{-1}.

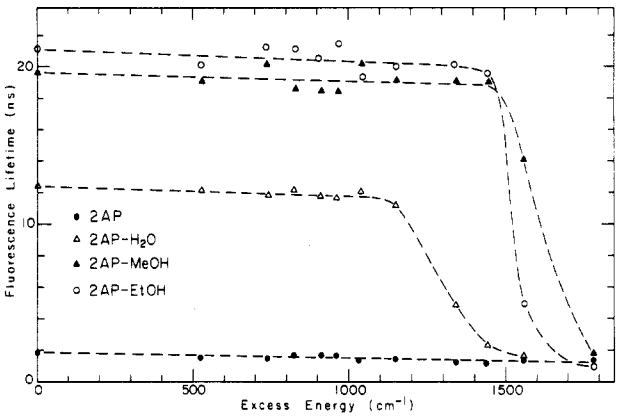

Figure 9. Plot of the fluorescence lifetimes vs. excess vibrational energy for the hydrogen-bonded 2AP complexes.

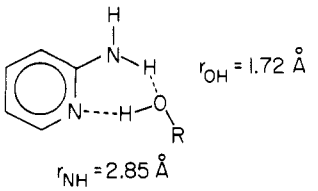

Figure 10. Calculated geometry from an atom–atom potential energy treatment of the planar 2AP–HOR hydrogen-bonded complexes. The bond lengths given in the figure are for 2AP–H_2O.

TABLE III: Complex Binding Energies (in cm^{-1})

complex	$\Delta\nu$	ΔIP	S_0	S_1	$\tilde{X}$
2AP–Ar	−32	−175[a]	<269	<301	<444
2AP–CH_4	−68	−368[a]	560–629	628–697	928–997
2AP–H_2O	−386	−3810[b]	~918	~1304	~4585
2AP–MeOH	−503	−4120[b]	~1007	~1510	~5090
2AP–EtOH	−518	−4020[b]	~992	~1510	~4970

[a] Experimental uncertainty of ±10 cm^{-1}. [b] Experimental uncertainty of ±~200 cm^{-1}.

We have also employed mass-selective one-color photoionization as an additional method for monitoring dissociation of these hydrogen-bonded complexes and a check of the fluorescence results. Here, complex ion production is monitored as a function of increasing S_1 vibrational energy. The onset of vibrational predissociation is indicated by a break off in the production of complex ion with a concomitant increase in the production of 2AP$^+$. For 2AP–H_2O dissociation was observed beginning at the 1304-cm^{-1} level and complete by 0 + 1433 cm^{-1}. For 2AP–MeOH and –EtOH, dissociation dominates beginning at the 1510-cm^{-1} band. These values are in good agreement with the fluorescence results.

Using the electronic spectral shifts and the excited-state binding energies, we can determine the ground-state hydrogen-bond strengths of these complexes from relationship 1 as illustrated above. Furthermore, estimates of the hydrogen-bonded complex ion binding energies can be made by utilizing the previously measured ΔIP values and relationship 2. Table III presents a summary of neutral complex ground- and excited-state bond strengths as well as values for the ground electronic state of the complex ions.

Table III demonstrates that these ionic hydrogen-bonded complexes are significantly more strongly bound than the neutral species: approximately 3 times more strongly bound. The additional stabilization is due to the charge–dipole and charge–induced dipole intermolecular interactions which become important for the complex ions.

2. Geometries of the Hydrogen-Bonded Complexes. We have calculated the hydrogen-bond interaction energies and geometries for 2AP–H_2O and 2AP–MeOH using atom–atom potentials.[8] The lowest energy planar configuration was found for a geometry in which there is neither a directed pyridine nitrogen lone pair of electrons nor a linear hydrogen bond. The equilibrium structure

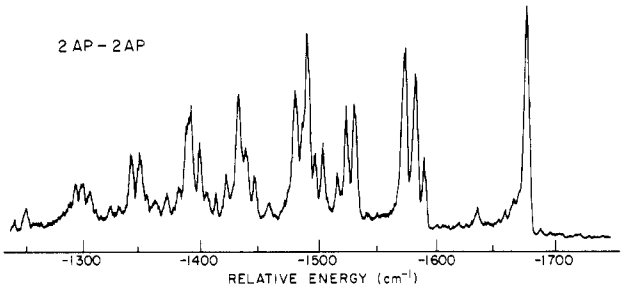

Figure 11. Mass-selected one-color photoionization spectrum of the low-energy electronic transitions of the 2AP dimer. Expansion conditions were P_0 = 3 atm of helium, D = 100 μm, and T = 49 °C.

for these two complexes is cyclic and is stabilized by two distorted hydrogen bonds. This structure is illustrated in Figure 10. Thus, in addition to the formation of the obvious O–H···N hydrogen bond between water and the pyridine lone electron pair, there is the possibility of the further complex stabilization through the formation of a second hydrogen bond between the inner amine hydrogen and the oxygen atom of the water molecule. The stronger of the two bonds was found to arise from the interaction of the oxygen atom with the amine hydrogen leading to a slightly shorter hydrogen bond distance compared with the N···HO bond. As one can see from Figure 10, both hydrogen bonds are distorted from the conventional linear arrangement, but the extra stabilization energy due to the formation of two hydrogen bonds more than compensates for the distortions. The calculated binding energies for the planar 2AP–H_2O and 2AP–MeOH complexes are 930 and 960 cm^{-1}, respectively.

These results are in good agreement with the planar geometry calculated by Del Bene[19] using ab initio SCF techniques with the STO-3G basis set. Del Bene reported[19] a 2AP–H_2O geometry with a cyclic configuration with two distorted hydrogen bonds. The formation energies of the complexes were found to be in the range of 1500–2000 cm^{-1}. The much larger binding energy in Del Bene's calculations compared with the present results is likely due to problems inherent to the STO-3G basis set as discussed by other authors.[20]

This planar geometry for 2AP–HOR should not be taken too seriously for the ground electronic state of the complex. As discussed above, the ground state of the 2AP monomer is nonplanar about the amino nitrogen with an out-of-plane angle of approximately 32°.[21] This leads to a double minimum potential for the inversion vibration in the ground electronic state.[21] Upon excitation to the $\tilde{A}$ state, it has been shown[11,12] that the monomer is planar or very nearly planar. Consequently, the ground electronic state of 2AP–H_2O is not expected to be planar, although the excited state of the complex however is likely planar. This geometry change in the $\tilde{A}$–$\tilde{X}$ transition will lead to excitation of a number of low-frequency intermolecular vibrations in the absorption spectrum. This is exactly what we have observed as illustrated in Table II by the low-energy intermolecular vibrational frequencies.

D. 2-Aminopyridine Dimer. At significantly lower energy than that required to excite the hdyrogen-bonded complexes discussed above, we have identified a series of previously unobserved absorption features. The intensities of these bands were found to be strongly temperature dependent and mass analysis following one- and two-color photoionization confirmed that these transitions are associated with the 2-AP dimer. Figure 11 displays the mass-selected photoionization spectrum of the dimer. The band origin of this system was measured to be 1668 cm^{-1} lower in energy than that of the monomer. This demonstrates a dramatic strengthening of the dimer bond(s) upon electronic excitation.

We have measured the fluorescence lifetimes of the 2AP dimer and have obtained further evidence of strong intermolecular interactions. The dimer lifetime is found to be 7.1 ns compared to the monomer value of 1.89 ns. Thus, similar to the water and alcohol complexes, hydrogen bonding in the 2AP dimer leads to a reduction in the efficiency of intersystem crossing manifested by a longer fluorescence lifetime than the isolated molecule.

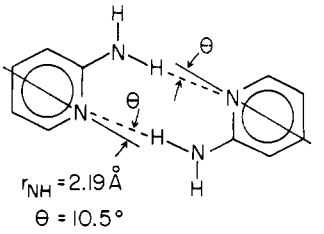

Figure 12. Calculated geometry from an atom–atom potential energy treatment of the planar 2AP dimer.

The spectrum shown in Figure 11 displays many low-frequency intermolecular vibrations, the most prominent of which are 7, 30, 45, 100, and 156 cm^{-1}. In order to aid in the understanding of this rather complicated spectrum, it is of use to explore the dimer geometry.

Atom–atom potential energy calculations show that the most stable dimer configuration is one in which two intermolecular hydrogen bonds are formed as illustrated in Figure 12. The dimer model is planar with C_{2h} symmetry, is characterized by hydrogen-bond lengths of 2.19 Å, and has a calculated binding energy of 1100 cm^{-1}.

Although this planar geometry may accurately represent the excited state of the dimer, it is certainly a simplification of the ground state as was discussed for the 2AP–HOR complexes. Consequently, in the ground state of the double hydrogen-bonded dimer, C_{2h} will not adequately describe the molecular symmetry. The excited state of the dimer, with two planar 2AP molecules, most likely is planar and thus C_{2h} is a good description.

The nonplanar-to-planar electronic transition will be characterized by a number of low-frequency transitions involving twists and torsions as well as the more common hydrogen-bond stretch and in- and out-of-plane bends. Considering these geometry changes of the 2AP dimer in the transtion to the $\tilde{A}$ state, one expects to observe an electronic spectrum dominated by low-frequency vibrations involving the intermolecular bonds. This is indeed what is observed in the spectrum in Figure 11. Furthermore, the planar nature of the excited state compared with the nonplanar-twisted ground state may be the source of the very large excited-state stabilization of the dimer as represented by the electronic spectral shift. A planar dimer will lead to much more linear hydrogen bonding, and possibly interaction between the respective π-electron distributions, and significantly stronger interactions. Additional investigations of the 2AP dimer are currently underway in our laboratory.

Conclusions

The electronic spectroscopy and excited-state dynamics of 2-aminopyridine complexes have been explored by using fluorescence and photoionization techniques. The complexing partners of interest in this study include argon, methane, water, methanol, and ethanol as well as the 2-aminopyridine dimer. The important results of these investigations are as follows:

1. Argon and Methane van der Waals Molecules. a. Bond Energies. The bond strengths of 2AP–Ar and –CH_4 have been determined for S_0, S_1, and the ground electronic state of the ionic complexes. The excited states of these complexes are stabilized by approximately 10% relative to the ground state of the neutral complexes, while the ionic ground states are ~60–70% more stable than the neutral ground states.

b. Vibrational Predissociation. When excited to the 0 + 824 cm^{-1} level, both complexes show predissociation rates slightly greater than the ionization rate. Furthermore, predissociation from this level appears to be a direct process occurring faster than extensive IVR of the complex. This results in the population of only a few fragment 2AP* vibrational levels at most. Excitation to the 0 + 967 cm^{-1} level, on the other hand, results in much more

(19) Del Bene, J. E. *J. Am. Chem. Soc.* **1979**, *101*, 7146.
(20) Honegger, E.; Bombach, R.; Leutwyler, S. *J. Chem. Phys.* **1986**, *85*, 1234.
(21) Kydd, R. A. *Spectrochim. Acta, Part A* **1979**, *35A*, 409.

extensive complex vibrational redistribution prior to dissociation leading to the population of a wide distribution of fragment 2AP* vibrational levels.

2. Hydrogen-Bonded Complexes: H_2O, MeOH, EtOH. a. Bond Energies. Changes of fluorescence lifetimes and one-color photoionization have been used to place upper limits on the hydrogen-bond energies of these complexes. Results show excited-state complex bond energies of approximately 1300 cm^{-1} for 2AP–H_2O and 1500 cm^{-1} for 2AP–MeOH and –EtOH. From electronic spectral shifts and ionization potential stabilization energies, hydrogen-bond energies for S_0 and $\tilde{X}^+$ have been determined. Ionic complexes have bond energies of about 3 times those of the excited-state neutral species.

b. Geometries. Calculations show that excited-state geometries of these complexes are probably planar and in a cyclic double bond arrangement. Ground-state geometries are likely more complicated due to the nonplanar nature of the 2AP molecule about the amino nitrogen atom. The nonplanar-to-planar geometry change upon electronic excitation is suggested to be the source of the high degree of excitation of intermolecular complex vibrations in our spectra.

3. 2-Aminopyridine Dimer. We have reported the electronic spectrum of the dimer of 2AP. The dimer shows a very large spectral shift of almost −1700 cm^{-1}. The geometry of the dimer has been suggested to be a double hydrogen-bonded arrangement involving an amino hydrogen and the pyridine lone electron pair on each monomer subunit. The large excited-state stabilization energy of the dimer may arise from the achievement of planarity in the excited state compared with a nonplanar-twisted geometry in the ground electronic state.

Acknowledgment. We acknowledge the financial support of the Natural Sciences and Engineering Research Council of Canada.

Registry No. 2AP, 504-29-0; H_2O, 7732-18-5; MeOH, 67-56-1; EtOH, 64-17-5; Ar, 7440-37-1; CH_4, 74-82-8.

NF($b^1\Sigma^+$) Quenching Rate Constants by Halogens and Interhalogens and the Excitation Rate Constant for IF(B) Formation

Hyungki Cha and D. W. Setser*

Chemistry Department, Kansas State University, Manhattan, Kansas 66506 *(Received: December 29, 1986; In Final Form: March 13, 1987)*

The flowing afterglow technique with Ar carrier gas (300 K) was used to measure the total quenching rate constants of NF($b^1\Sigma^+$) by halogen and interhalogen molecules. The NF($b^1\Sigma^+$) radicals were prepared by the dissociative excitation-transfer reaction between Ar($^3P_{0,2}$) metastable atoms and NF_2. The quenching rate constants, which are in the (0.35–15) × 10^{-11} cm^3 $molecule^{-1}$ s^{-1} range, increase with molecular weight of the halogens. In the reaction zone the NF(b) vibrational distribution was v_0'–v_3' = 1.00:0.24:0.14:0.09; however, there was no obvious dependence of the quenching rate constants on v'. The excitation rate constant for IF($B^3\Pi_{0^+}$) formation from NF(b), with a v_0'–v_3' distribution of 1.00:0.14:0.08:0.04, was measured as (1.4 ± 0.2) × 10^{-12} cm^3 $molecule^{-1}$ s^{-1}, which corresponds to a branching fraction of about 0.02. The only other reaction that gave emission was I_2 with a similarly small $I_2(B^3\Pi_{0_u^+})$ formation branching fraction. Qualitative measurements of the quenching rate constants for I atoms, CN radicals, ICN, and BrCN were obtained.

Introduction

Efficient excitation-transfer reactions between a metastable species and a suitable acceptor molecule are of current interest because of possible applications to new laser systems. The success of the oxygen–iodine laser[1] has encouraged study of NF, which is isoelectronic with O_2 but with higher energy metastable states. The NF($a^1\Delta$) (11 435 cm^{-1}) and NF($b^1\Sigma^+$) (18 905 cm^{-1}) states, with lifetimes of 5.6 s and 20 ms, respectively,[2,3] can be studied by flowing afterglow techniques. Halogens and interhalogens are possible acceptors for NF(b) because the energy of NF(b) is sufficiently high that several halogen excited states can be produced. The IF system is particularly interesting because the IF($B^3\Pi_{0^+}$) state is one of the more stable excited states[4] and is in energy resonance with NF(b,v'=0).

$$NF(b^1\Sigma^+,v'=0) + IF(X^1\Sigma^+,v''=0) \rightarrow NF(X^3\Sigma^-,v''=0) + IF(B^3\Pi_{0^+}, v'=0);\ \Delta H^\circ_0 = 48\ cm^{-1} \quad (1a)$$

$$\rightarrow \text{other products} \quad (1b)$$

The radiative and quenching properties of the IF(B) state have been studied,[4-9] and the feasibility of an electronic transition laser operating on the B–X transition has been demonstrated.[10,11] Energy transfer from NF(b) to IF(X) has been reported,[12] but quantitative studies are needed to ascertain the efficiency.

This laboratory has developed a flowing afterglow source of NF(b,$v'\leq 3$) that is based upon the NF_2 + Ar($^3P_{0,2}$) reaction.[3] This technique has been shown to be suitable for measurement of quenching rate constants, and in this work the method was adapted for a comprehensive study of NF(b) quenching by halogens. The total quenching rate constants at room temperature were measured

(1) (a) McDermott, W. E.; Pchelkin, N. R.; Benard, D. J.; Bousek, R. R. *Appl. Phys. Lett.* **1978**, *32*, 469. (b) Benard, D. J.; McDermott, W. E.; Pchelkin, N. R.; Bousek, R. R. *Appl. Phys. Lett.* **1979**, *34*, 40. (c) Bachar, J.; Rosenwaks, S. *Appl. Phys. Lett.* **1982**, *41*, 16.
(2) Malins, R. J.; Setser, D. W. *J. Phys. Chem.* **1981**, *85*, 1342.
(3) Lin, D.; Setser, D. W. *J. Phys. Chem.* **1985**, *89*, 1561.
(4) Clyne, M. A. A.; McDermid, I. S. *J. Chem. Soc., Faraday Trans. 2* **1976**, *72*, 2242.
(5) Clyne, M. A. A.; Coxon, J. A.; Townsend, L. W. *J. Chem. Soc., Faraday trans. 2* **1972**, *68*, 2134.
(6) Clyne, M. A. A.; McDermid, I. S. *J. Chem. Soc., Faraday Trans. 2* **1976**, *72*, 2252.
(7) Clyne, M. A. A.; McDermid, I. S. *J. Chem. Soc., Faraday Trans. 2* **1977**, *73*, 1094.
(8) Clyne, M. A. A.; McDermid, I. S. *J. Chem. Soc., Faraday Trans. 2* **1978**, *74*, 1644.
(9) (a) Davis, S. J.; Hanko, L.; Shea, R. F. *J. Chem. Phys.* **1983**, *78*, 172. (b) Wolf, P. J. Ph.D. Dissertation, Air Force Weapons Lab, 1984.
(10) Wolf, P. J.; Glover, J. H.; Hanko, L.; Shea, R. F.; Davis, S. J. *J. Chem. Phys.* **1985**, *82*, 2321.
(11) Davis, S. J.; Hanko, L.; Wolf, P. J. *J. Chem. Phys.* **1985**, *82*, 4831.
(12) (a) Pritt, A. T. Jr.; Patel, D.; Benard, D. J. *Chem. Phys. Lett.* **1983**, *97*, 471. (b) Pritt, A. T.; Benard, D. J. In *Gas-Phase Chemiluminescence and Chemiionization*; Fontijn, A., Ed.; North-Holland: Amsterdam, 1985; Chapter 15. (c) Pritt, A. T. Jr.; Benard, D. J. *J. Chem. Phys.* **1986**, *85*, 7159.
(13) Trickl, T.; Wanner, J. *J. Chem. Phys.* **1983**, *78*, 6091.

0022-3654/87/2091-3758$01.50/0